QUASI-FREE (p,pα) SCATTERING ON
^{24}Mg, ^{28}Si, ^{40}Ca AND ^{58}Ni AT 157 MeV.

D. BACHELIER, J.L. BOYARD, T. HENNINO,
H.D. HOLMGREN, J.C. JOURDAIN,
P. RADVANYI, P.G. ROOS and
M. ROY-STEPHAN.

IPNO-PhN-76-05

QUASI-FREE (p,pα) SCATTERING ON ^{24}Mg, ^{28}Si, ^{40}Ca AND ^{58}Ni AT 157 MeV.

D. Bachelier, J.L. Boyard, T. Hennino, H.D. Holmgren[(+)], J.C. Jourdain[(++)], P. Radvanyi, P.G. Roos[(+)] and M. Roy-Stephan

Institut de Physique Nucléaire, BP n°1, 91406 - Orsay (France).

Abstract

Sixfold energy spectra have been measured for the (p,pα) reaction at 157 MeV on ^{24}Mg, ^{28}Si, ^{40}Ca and ^{58}Ni around quasi-free kinematic conditions. For the three s-d shell nuclei the experiment covered a map ranging from 0 to 220 MeV/c in recoil momentum and from 0 to 20 MeV in excitation energy of the final nucleus. Recoil momentum distributions have been obtained for the 0^+ ground state and the 2^+ first excited state of ^{20}Ne, ^{24}Mg and ^{36}A, and also for the states around 4.4 MeV (mainly 4^+) of ^{36}A. The α spectroscopic factors extracted by a DWIA analysis are about 3 times larger than those predicted by the SU(3) model ; however, they agree quite well in relative magnitude for a number of cases. The disagreement in shape between experiment and theory observed at low recoil momentum for the 2^+ states might result from another reaction mechanism. The cross-sections for ^{58}Ni are about a factor of 10 smaller than those for ^{40}Ca. The $^{58}Ni(p,p\alpha)^{54}Fe$ reaction seems to lead mainly to excited states of the final nucleus.

NUCLEAR REACTIONS ^{24}Mg, ^{28}Si, ^{40}Ca, $^{58}Ni(p,p\alpha)$, E = 157 MeV, measured $\sigma(E_p, E_\alpha, \theta_p, \theta_\alpha)$; deduced reaction mechanism ; extracted α spectroscopic factors, compared with SU(3) predictions. Enriched ^{24}Mg and ^{58}Ni targets.

(+) On leave from University of Maryland, Department of Physics and Astronomy, College Park, Maryland, U.S.A.

(++) This work is part of the Doctorat d'Etat thesis of J.C. Jourdain (Université Paris-Sud, Centre d'Orsay) 1976.

1 - Introduction

For some time, the possible α-structure of nuclei has been one of the intriguing problems of nuclear structure. Cluster models, especially α particle models for light nuclei, have been devised and numerous calculations have been carried out. It has often been stated that the observation of alpha particles emerging from a nucleus does not mean that these alpha particles exist as such inside the nucleus. A realistic shell model does predict non negligible α-parentages [1]. The recent quartet description [2] stresses the importance of 2p2n groups inside nuclei. Moreover, it has been suggested [3] that the surface of nuclei might be particularly rich in α-particle like structures.

In order to obtain more quantitative information on α clustering in nuclei, we have chosen to study the (p,pα) reaction on several even-even nuclei in the region of the kinematic conditions corresponding to free p-α scattering. Similar information may also be obtained from other reactions. For example 2p2n transfer reactions are complementary to the quasi-free (p,pα) reaction ; however, their analysis is somewhat more involved, requiring the use of finite range and heavy ion optical potentials. Recently, attention has also focused on measurements of γ ray spectra associated with absorption of pions, kaons and high energy protons in nuclei [4] ; however, in such integral measurements, the analysis is much more indirect and cannot exclude cascades of sequential proton and neutron emissions resulting from the characteristics of the levels of the intermediate and final nuclei.

The kinematic conditions for a (p,pα) reaction are represented in fig.1. Energy and momentum conservation can be written as

$$E_s = E^* + Q = E_o - E_p - E_\alpha - E_R \qquad (1a)$$

$$\vec{q}_R = \vec{p}_o - \vec{p} - \vec{p}_\alpha \qquad (1b)$$

where E_s is the separation energy of the knocked-out alpha-particle; the subscript R denotes the recoil nucleus ; E^* is the excitation energy of the recoil nucleus. The other notations are given in fig.1.

In the plane wave impulse approximation (PWIA) one has $\vec{q} = -\vec{q}_R$, where $\vec{q}$ is the *momentum of the center of mass of the four knocked-out* nucleons in the target nucleus before the interaction. The quasi-free (p,pα) reaction can be then visualized by the diagram shown in fig.2.

In a coplanar geometry, coincidence measurements lead to the cross sections $d^4\sigma/d\Omega_p\, d\Omega_\alpha\, dE_p\, dE_\alpha$. The two most interesting variables are E^* (or E_s) and $\vec{q}_R$. If one further integrates in energy over the width of a specific final state of the recoil nucleus, one can write in PWIA, assuming that the group 2p2n in the diagram of fig.2 has characteristics very close to those of a free alpha-particle [1,5],

$$d^3\sigma/d\Omega_p\, d\Omega_\alpha\, dE = K\left[\frac{d\sigma}{d\Omega}\right]_{\substack{free\\(p+\alpha)}} \sum_{N,L} S_{NL}\, P_{NL}\,(q) \qquad (2)$$

where K is a kinematic factor ; $\left[\frac{d\sigma}{d\Omega}\right]_{\substack{free\\(p+\alpha)}}$ is the free p-α elastic cross-section [6] in kinematic conditions as "close" as possible to those of the (p,pα) reaction, which involves the usual ambiguities of the impulse approximation ; S_{NL} is a spectroscopic factor corresponding to an α-cluster with quantum numbers N,L in the initial nucleus, and $P_{NL}(q)$ is the normalized momentum distribution of this α-cluster. There will be only one value of L if the target nucleus has J=0.

If no distorsion were present, we would be able to extract S_{NL} directly from the experimental data by performing the integral $4\pi\, S_{NL} \int P_{NL}(q)\, q^2\, dq$. However, there is always distorsion, and one measures a distorted momentum distribution. Thus a more sophisticated theoretical treatment such as the DWIA [7,8] is necessary to extract S_{NL}. An alternative to the DWIA is the separate calculations of graphs of higher order [9] than the one shown in fig.2.

In the (p,pα) experiment two kinds of distributions are measured:

a) Total energy spectra or excitation energy spectra of the residual nucleus (which are related by expression 1a) corresponding to a certain interval of $|\vec{q}_R|$ in order to identify the final states of the recoil nucleus.

b) Recoil momentum distributions for the various final states, for kinematic conditions around $\vec{q}_p = \vec{0}$.

If the leading reaction mechanism is the one represented in fig.2, one expects these momentum distributions to show, near $\vec{q}_R = \vec{0}$, a maximum for L=0 and a minimum for L≠0. This measurement of the momentum distribution can be performed by varying θ_α or θ_p (angular correlation), or by varying the ratio E_p/E_α (energy sharing). In the choice of the kinematic conditions, outgoing alpha-particles (or protons) should have enough energy in order to minimize the possible sequential mechanisms. To achieve this, the incident energy has to be sufficiently high. Experimental data of this type provide information on the reaction dynamics, and a DWIA analysis should permit the extraction of the spectroscopic factors which can then be compared with the predictions of nuclear models.

One might raise the question as to whether the quasi-free scattering formalism should be extended to situations where the four knocked-out nucleons did not have the characteristics of a free alpha-particle in the target nucleus [10]. In this case, the summation in expression (2) must be extended and the appropriate spectroscopic factors and P(q) distributions included. In addition, the free p-α elastic cross-section must then be replaced, inside the summation, by a corresponding inverse inelastic (break-up) cross section. If the internal quantum numbers of the group of four nucleons (in the intermediate state of fig.2) are different from J=0, T=0 inside the initial nucleus, this might be identified through the quantum numbers of the states excited in the final nucleus.

Relatively few experiments have been performed on (p,pα) scattering. Some of these have been done at low energies or have been restricted to 1p shell nuclei [11]. The (p,pα) cross section drops by about two orders of magnitude from ^{6}Li to ^{24}Mg at 157 MeV [12]. Up to now, the higher energy experiments did not resolve the individual final states [13].

A previous quasi-free (p,pα) scattering experiment [12], performed for a limited set of kinematic conditions, gave us some energy spectra and reaction cross sections for the α knock-out process. However, the recoil momentum varied continuously along each energy spectrum. Thus we extended our detection system in order to cover kinematically not only two strips in the $(E^*, |\vec{q}_R|)$ space, but a map ranging from 0 to 20 MeV in E^* and from 0 to 220 MeV/c in $|\vec{q}_R|$, for three 4n target nuclei of the s-d shell (^{24}Mg, ^{28}Si and ^{40}Ca) and one heavier even-even target nucleus (^{58}Ni).

2 - Experimental method and set-up

2.1 The $(E^*, |\vec{q}_R|)$ map.

A combination of the energy sharing and the angular correlation methods, with 5 detector telescopes (two for the alphas and three for the protons) was used in order to obtain 6 simultaneous spectra. The experimental set-up is presented in fig.3. The θ_p angle, the two θ_α angles and the three Ep energies where fixed for each measurement. The θ_α angles and the distances between the proton detectors in the focal plane of the magnetic spectrometer were set so as to obtain an experimental value every 25 to 30 MeV/c at constant E^*, and the experimental points close to $|\vec{q}_R|=0$ every 4 MeV in E^*.

With two such sixfold measurements, we covered the $(E^*, |\vec{q}_R|)$ map for each target. Such a map is shown in fig.4 for ^{28}Si. Each curve corresponds to an elementary energy spectrum ; i.e., a combination of one proton and one alpha detector. The slope of each $|\vec{q}_p|$ (E^*) kinematic curve is related to the recoil angle θ_R. Thus, we notice in the polar coordinate representation (fig.4) that the recoil direction changes drastically for spectra corresponding to small $|\vec{q}_R|$ values. Curves with opposite slopes at the same $(E^*, |\vec{q}_R|)$ point provide information on the symmetry of the quasi-free scattering process about $\vec{q}_R = \vec{0}$.

2.2 Choice of the experimental conditions

For a fixed θ_p angle, the E_p energies were chosen so as to include in each telescope 1 spectrum the $|\vec{q}_R| \approx 0$ condition for selected values of E^*. Because of the relatively small variations in E_p during the experiment, the momentum transferred to the scattered proton was nearly constant. Since in the impulse approximation (PWIA or DWIA) the quasi-free cross section should be proportional to the free cross section, one may tend to decrease θ_p in order to have sizeable counting rates. However, this leads to a decrease in E_α and an increase in distorsion effects. It also increases the importance of sequential processes which were noticed in our previous experimental spectra [12] for high excitation energies and large $|\vec{q}_R|$ values. We also needed to cover a sufficient range in E_α energies. As a compromise, we have chosen $\theta_p = 50°$ (except for some special measurements) and the energies of the detected α particles varied from 15 to 60 MeV in the experiment. Table 1 gives a description of the different measurements made for each target.

The energy and recoil momentum resolutions are directly related to the width Δy of the proton detectors in the magnet focal plane, to the target thickness, to the solid angles $\Delta\Omega_\alpha$ and $\Delta\Omega_p$, and to the primary beam energy width. These different factors also fixed the counting rate which had to be increased as much as possible, because of the very low cross sections. The accidental rate presented the main limitation. The proton detector widths were fixed at $\Delta y = 6$ cm (which gave $\Delta E_p \simeq 1.7$ MeV at $E_p = 100$ MeV), and the target thicknesses were between 10 and 15 mg.cm^{-2}. This, with a 1 MeV (FWHM) primary beam width, led to an average excitation energy resolution $\Delta E \gtrsim 2.6$ MeV (FWHM) and an average recoil momentum resolution $\Delta|\vec{q}_R| \gtrsim 30$ MeV/c (FWHM), with solid angles $\Delta\Omega_\alpha = 2.4\ 10^{-3}$ sr and $\Delta\Omega_p = 1.7\ 10^{-3}$sr.

2.3. Beam. Monitoring. Targets.

In order to reduce the rate of accidental coincidences and the pile up in the detectors, we used the 157 MeV proton beam of the Orsay synchrocyclotron with the auxiliary extraction, giving a 15 to 20% duty cycle and an average intensity of 10 nA. A helium ionisation chamber, calibrated with a Faraday cup, was used as monitoring device. Table 2 gives a description of the different targets used and the resolution obtained : ^{4}He (for calibration), ^{24}Mg, ^{28}Si, ^{40}Ca, ^{58}Ni. The target angle was chosen so as to minimize the energy loss for the emitted alpha particles.

2.4. Detection, Electronics, Identification of alpha particles.

After passing through a 6.0 cm wide and 5.5 cm high diaphragm the protons were deflected by a magnetic spectrometer of 1.7 m radius and 120° deflecting angle. In the focal plane of the magnet, they were detected and identified by three range telescopes. Each telescope consisted of two coincident scintillation counters separated by a 10 mm thick aluminium absorber that stopped particles less penetrating than protons. The first plastic scintillator was 6 cm wide. Alpha particles were detected and identified by two ΔE-E telescopes situated in the vacuum of the reaction chamber and separated by 15°. Each telescope consisted of two silicon detectors cooled to -25°C by a Peltier cell. Small permanent magnets placed just in front of the circular entrance slits prevented secondary electrons from reaching the solid state detectors. The slits were 12 mm in diameter and placed 20 cm from the target. The ΔE and E detectors were 100 μm and 1.5 mm thick respectively.

The proton scintillators were coupled to 56 AVP photomultipliers, followed by fast coincidence circuits, which generated the start signals for two time to amplitude converters (TAC) corresponding to the two alpha particle telescopes. Each ΔE-E α particle telescope was followed by conventional electronic circuits, with a ΔE constant fraction discriminator to provide the stop signal for the TAC. The TACs were operated on a 200ns range, allowing the inclusion of three RF bursts of the machine (bursts separated by 49.5 ns), one of them including the real p-α coincidences, and two others allowing the evaluation of the accidental rate.

The ΔE and E linear pulses, as well as the time of flight pulses produced by the TACs, were fed into a 370-135 IBM Computer (ARIEL) through a set of analog to digital converters. Each 32-bit word corresponding to one event included four bits indicating which of the three proton telescopes (A, B or C) and which of the two alpha telescopes (1 or 2) had been triggered by the coincidence. Most unwanted events were rejected electronically ; i.e., by the settings of the constant fraction discriminator thresholds, the gates and coincidence circuits. The event words were stored on a magnetic disk of the computer and treated on-line in order to provide a running display of the accumulated data. For each α-telescope, the alpha particles were identified on a $(\Delta E, E)$ map and separated by specifying two border-lines with the help of the computer. The alpha particle spectra were then obtained by projection onto the E axis. Each measurement was divided into several three hour-long runs.

In the time of flight spectrum, all alpha particles appeared in a narrow interval of 7 ns. Narrow limits ($\sim$10ns) could thus be fixed, thereby reducing the accidental coincidences to a few per cent of the true coincidences.

2.5. Experimental calibration.

Before starting the $(p,p\alpha)$ measurements, several calibrations were performed. The different time delays, the angles and the energies were adjusted and calibrated by means of a free p-α elastic scattering experiment on a gaseous ^4He target. The ^4He gas was contained at 2 atm. pressure in a 1 cm diameter havar cylinder. This calibration was made at θ_p = 46., 60. and 71. degrees.

In order to obtain a standard $(\Delta E, E)$ map allowing easy identification and separation of the various particles, several singles spectra were obtained with the two solid state detector telescopes. This procedure easily permitted the selection of the two limiting lines for the alpha particle region.

2.6. Evaluation and analysis of the events.

An average 3-hour long run produced, for the s-d shell nuclei, 10^7 singles in Telescope 1, 10^4 singles events in Detector B, and 100 events in the 200 ns TAC range for the coincidence B1. After separation by time and alpha particle identification, this example gave 12 real and 1 accidental $p,p\alpha$-events. In this way, we had about one $p,p\alpha$-event every three minutes for the whole detection system, and the accidental rate in the energy region $E^* < 5$ MeV was generally less than 5%. About 20 such 3-hour runs were taken for each target at a given angular setting.

3 - Experimental results

From the summed excitation energy spectra obtained by averaging $d^4\sigma/dE_p\, d\Omega_p\, dE_\alpha\, d\Omega_\alpha$ over a particular interval of $|\vec{q}_R|$ in the $(E^*, |\vec{q}_R|)$ map we can identify the first states excited in the $(p,p\alpha)$ reaction, even with the poor energy resolution. Then, we use the elementary spectra to extract $d^3\sigma/dE_p\, d\Omega_p\, d\Omega_\alpha$ for the states which have been identified, either by a fitting procedure when statistics are sufficient, or by a simple separation cut when they are poor. Finally, having chosen a unique way to define the sign of the variable q_R, we present $d^3\sigma(q_R)$ distributions from which the α-spectroscopic factors can be extracted by a DWIA analysis.

3.1. Averaged excitation energy spectra.

In order to analyze the relative importance of the final states as $|\vec{q}_R|$ increases, we have extracted summed energy spectra from the $(E^*, |\vec{q}_R|)$ map, averaging the cross section over the $|\vec{q}_R|$ intervals 0-220, 0-100, and 100-220 MeV/c (figs. 5,6 and 7). For ^{40}Ca, an additional averaged energy spectrum has been extracted for a narrow 60-90 MeV/c interval, which corresponded to a special sixfold measurement performed in order to compare the first 2^+ state to the 0^+ g.s. in this region : i.e., kinematic conditions were chosen so that, for these states, $|\vec{q}_R|$ fell in this interval for all six measurements.

For the three s-d shell nuclei, the $d^4\sigma/dE_p\, d\Omega_p\, dE_\alpha\, d\Omega_\alpha$ averaged spectra show strongly excited low lying states. In addition there exists a minimum around 4.5 MeV excitation for ^{24}Mg and ^{28}Si (fig.5) and around 7 MeV for ^{40}Ca (fig.6). For this limited ground state region, the cross section $d^3\sigma/dE_p\, d\Omega_p\, d\Omega_\alpha$ is about the same for ^{24}Mg and ^{40}Ca and about a factor of two smaller for ^{28}Si. The summed energy spectrum for the ^{58}Ni target (fig.7) shows a quite different behaviour, with a very small cross section for the ^{54}Fe ground state region below 4.5 MeV. For all spectra, sequential processes appear as E^* and $|\vec{q}_R|$ become larger than 10 MeV and 90 MeV/c respectively.

For all three s-d shell nuclei the 0^+ g.s. clearly dominates the 0-100 MeV/c spectrum. However, the first 2^+ state is relatively important for both ^{24}Mg and ^{40}Ca. In the 100-200 MeV/c band the first 2^+ state becomes comparable to the 0^+ g.s. for all three of these nuclei. This increased importance of the 2^+ state for large $|\vec{q}_R|$ is as expected, since the L=2 momentum distribution is broader than that for L=0. For ^{40}Ca, a peak appears near 4.4 MeV excitation energy which is as strong as the 2^+ state in the low momentum band, and twice as strong as the 2^+ state in the high momentum band. This behaviour suggests an important contribution from the 4^+ state in the corresponding $(0^+,2^+,4^+)$ group of states in ^{36}A. The 50-90 MeV/c band shows comparable values for the three peaks (fig.6).

3.2. Elementary excitation energy spectra.

For each of the low energy states mentioned, a value of $d^3\sigma/dE_p\,d\Omega_p\,d\Omega_\alpha$ has then been extracted from each elementary spectrum. When the statistics were too poor, a separation was made by a simple cut at the mean energy between two neighbouring states, and at values corresponding to the experimental resolution in E^* for the upper and lower limits. When more than 20 events had been accumulated in an elementary spectrum for a single state, a fitting procedure was used. Each state was represented by a Gaussian distribution with a FWHM defined by the experimental resolution in E^*. The cross sections $d^3\sigma/dE_p\,d\Omega_p\,d\Omega_\alpha$ were then obtained after normalization of the sum of the gaussian areas to the data. As the statistics are generally quite poor in these (p,pα) experiments, especially at large $|\vec{q}_R|$, only 10 spectra, out of the 51 spectra obtained for the three nuclei ^{24}Mg, ^{28}Si and ^{40}Ca, could be analysed by this fitting procedure. Because of the very low cross section for ^{58}Ni, only an energy spectrum integrated over the whole range of $|\vec{q}_R|$ is shown for this nucleus (fig.7).

Some elementary excitation energy spectra are shown in fig.8. The cross section corresponding to the ground state region decreases by about two orders of magnitude from ^{6}Li to ^{24}Mg, ^{28}Si and ^{40}Ca, and three orders of magnitude from ^{6}Li to ^{58}Ni. The $d^3\sigma/dE_p\,d\Omega_p\,d\Omega_\alpha$ obtained for $|\vec{q}_R|(0^+) \gtrsim 0$ show a very prominent 0^+ ground state for ^{24}Mg, ^{28}Si and

^{40}Ca. At large $|\vec{q}_R|$, the 2^+ first excited state dominates for ^{24}Mg and ^{28}Si, while the 4.4 MeV peak dramatically dominates for ^{40}Ca.

When integrated over the first 5 MeV of excitation energy, these results agree with our previous experiment [12] where the cross section $d^3\sigma/dE_p\, d\Omega_p\, d\Omega_\alpha$ could only be given for the whole group of states below 5 MeV for two values of $|\vec{q}_R|$.

3.3. Distributions $d^3\sigma(q_R)$.

Experimental results corresponding to the different kinematic conditions (i.e., different measurements) are presented in figs.9 to 11, for ^{24}Mg, ^{28}Si and ^{40}Ca. We have plotted $d^3\sigma/dE_p\, d\Omega_p\, d\Omega_\alpha$ versus the recoil momentum q_R, where $q_R \equiv |\vec{q}_R| \dfrac{\vec{q}_R\cdot\vec{p}_\alpha}{|\vec{q}_R\cdot\vec{p}_\alpha|}$ is an algebraic variable corresponding uniquely to the vector $\vec{q}_R$, and having $|\vec{q}_R|$ as absolute value. In our experiment the vector $\vec{q}_R$ has the simple geometrical property illustrated in figs.1 and 4; viz. its endpoint follows a straight line parallel to the direction of the detected α particles. The magnitude $|\vec{q}_R|$ is double valued for such a line, the two solutions corresponding to different directions of $\vec{q}_R$. In order to distinguish these two possibilities in a plot of $d^3\sigma$ versus $\vec{q}_R$, we have chosen the sign convention above, which of course is somewhat arbitrary, but reflects the variation of θ_R. The distorsion, however, has been calculated separately for each $\vec{q}_R$, and the comparison with DWIA is free from this arbitrariness. The way we have defined q_R is in agreement with the Maryland representation [14] where E_p increases with q_R for a given set of angular conditions ; the sign of q_R is the same as that of $\dfrac{\partial|\vec{q}_R|}{\partial E^*}$, the slope of the kinematic curve $|\vec{q}_R|(E^*)$ on the $(E^*, |\vec{q}_R|)$ map (fig.4).

As distorsion effects are different for each measurement and each telescope (i.e. each spectrum), we do not expect a continuous curve for the display of the various results for a given final state. This is the reason why only sets with definite values for θ_α and θ_p give series of 3 points (corresponding to three different E_p separated by approximately 3.5 MeV) related to one DWIA curve. Notwithstanding, the general features of the distribution obtained show a common behaviour for

$d^3\sigma(q_R)$, as can be seen in fig.9 to 11 and in table 3 :

- the experimental distributions show the typical L=0 bell shape for the 0^+ ground states, whereas the 2^+ first excited states exhibit a L≠0 shape, but without any pronounced minimum at $q_R = 0$.

- the distribution of the 4.4 MeV group for ^{40}Ca is rather flat and contains large momentum components.

0^+ ground states.

The maximum of the L=0 distribution appears at q_R=0 for ^{28}Si (fig.10) but is somewhat shifted toward negative values of q_R for ^{24}Mg (fig.9) and ^{40}Ca (fig.11). The absolute value of the cross section at this maximum is nearly the same for ^{24}Mg and ^{40}Ca but about 30% smaller for ^{28}Si. The apparent FWHM is about 100 MeV/c for ^{28}Si and ^{40}Ca and somewhat smaller for ^{24}Mg.

In order to compare distorsion effects in different experimental conditions, a third measurement was made for ^{24}Mg and ^{40}Ca, covering the same $|\vec{q}_R|$ (E^*) kinematic curve as in the first measurement. The measurement corresponded to different angular (θ_α -3.4° ; θ_p +7.3°) and energy (E_p -6.9 MeV) conditions. For the same $|\vec{q}_R|$, the results show a decrease in $d^3\sigma(q_R)$ of a factor $2.6^{+1.4}_{-0.8}$ for ^{24}Mg and $1.3^{+0.4}_{-0.3}$ for ^{40}Ca (see table 3).

2^+ first excited states.

In no 2^+ case is there a clear-cut minimum expected for an L≠0 distribution, although the ^{28}Si distribution shows some slight evidence. Thus the minima must be completely filled in by distorsion or other effects such as those discussed in our conclusions. The magnitude of $d^3\sigma(q_R)$ is quite small, less than 1 $\mu b.MeV^{-1}.sr^{-2}$. The cross sections for ^{24}Mg and ^{28}Si are comparable, and that for ^{40}Ca is about twice as large (see table 3). If one ignores the lack of a minimum and intreprets the results in terms of an L≠0 distribution, the maximum of the distributions would be located near q_R = ~ 130 MeV/c. In addition, the distributions are broad (FWHM ≈ 250 MeV/c). These two results are consistent with expectations for an L≠0 distribution.

The "4.4 MeV" group of excited states for the ^{40}Ca target

The results (fig.11) show a maximum value of about $1\mu b.MeV^{-1}.sr^{-2}$ for $d^3\sigma(0)$, which in this case might be due to the contribution of the 0^+ component of the group $(0^+,2^+,4^+)$, as well as effects mentioned above for the 2^+ states. The maxima which would correspond to a $L\neq 0$ distribution appear around ±130 MeV/c. The very large FWHM of about 320 MeV/c (much larger than the 2^+ FWHM) seems to indicate a dominant 4^+ contribution at large values of $|\vec{q}_R|$.

4 - DWIA Analysis

The experimental data have been compared to Distorted Wave Impulse Approximation (DWIA) calculations in order to extract more detailed spectroscopic information. In the DWIA the expression for the theoretical (p,pα) cross section has the same form as in the PWIA (eq.2, Sect.1) with the exception that the P(q) now becomes the distorted momentum distribution. In particular the distorted momentum distribution $P_{NL}^{DW}(q)$ is defined [14,15] as $P_{NL}^{DW}(q) \propto \sum_M |T_{NL}^M(q)|^2$, with

$$T_{NL}^M(q) = (2L+1)^{-1/2} \int \chi_{k_p}^{(-)*}(\vec{r})\ \chi_{k_\alpha}^{(-)*}(\vec{r})\ U_{NL}^M(\vec{r})\ \chi_{k_o}^{(+)}(\gamma\vec{r})\ d\vec{r}$$

where $\chi_{k_o}^{(+)}$, $\chi_{k_p}^{(-)}$ and $\chi_{k_\alpha}^{(-)}$ represent the distorted waves for the incoming proton, the outgoing proton, and the outgoing α particle, respectively. γ is the quantity $\frac{M_A-M_\alpha}{M_A}$ where M_A is the target mass and M_α the alpha particle mass. The wave function $U_{NL}^M(\vec{r})$ describes the motion of the center of mass of the α cluster in the target nucleus, and as such, represents a complicated overlap integral between the target nucleus wave function and the product of the residual nucleus and alpha particle internal wave functions.

The DWIA calculations were carried out with the code of N.S. Chant [6]. The code generates the distorted waves by solving the

Schrödinger equation for Woods-Saxon optical potentials, excluding spin-orbit effects, using a partial wave expansion (24 to 30 partial waves were included for each channel in order to insure accuracy to sufficiently large radii). For the present calculations, the proton optical potentials were taken from the analysis of Comparat et al.[16] of 155 MeV proton elastic scattering. The well depths were changed somewhat for the outgoing proton channel to account for the energy dependence of the proton optical potential. For the α channel, most of the calculations were carried out with optical potentials characterized by real well depths of around 100 MeV. For $^{24}Mg(p,p\alpha)^{20}Ne$ the α potential was taken from Singh et al.[17] who analyzed 40 and 50 MeV α elastic scattering on ^{24}Mg. The same potentials were used for $^{28}Si(p,p\alpha)^{24}Mg$. The $^{40}Ca(p,p\alpha)^{36}A$ α potential was obtained from the work of Chang and Ridley[18] who investigated α elastic scattering on ^{40}Ca over the energy range from 20 to 80 MeV. The potentials are listed in table 4. Other α potentials were tried and their effects are discussed below.

As stated previously, the wave function $U_{NL}(\vec{r})$ actually represents a complicated overlap integral. In the calculations $U(\vec{r})$ was obtained by binding an α particle in a Woods-Saxon well with the appropriate α particle separation energy. For the 2s-1d shell, based on oscillator quanta, the wave function was assumed to be a 5S state for L=0 knock-out and a 4D state for L=2 knock-out. The appropriateness of this treatment is rather questionable, particularly for the wave function inside the nucleus. However, it does have the desirable feature that the asymptotic tail is determined by the α-particle separation energy - an important feature in the present calculations. Even having chosen this method to replace the overlap integral one is left with the choice of the Woods-Saxon potential geometry. We have chosen a well geometry similar to that obtained from elastic α scattering. The effects of changes in the geometry will be discussed later.

The calculations are compared directly to the experimental data in the next section. In this section we investigate typical distortion effects, and the sensitivity of the calculations to various ingredients. One can see a comparison between DWIA and PWIA in table 3 and fig. 13. First one observes that the distortion dramatically reduces the magnitude of P(q) at small recoil momentum as evidenced by the normalization factor required, emphasizing the strong absorption characteristics of the reaction. Secondly, for the L=0 transition the distorted momentum distribution is significantly broader than that for plane waves, and the minima present in the PWIA calculations at about 120 MeV/c due to the 5S nature of the wave function are completely filled in by distortion effects. Thirdly, we observe that the distortion effects tend to shift the maximum of the L=0 distribution by about 10 MeV/c to somewhat lower q_R values. Finally, we see that the large differences between the L=0 and L=2 magnitudes at small recoil momentum are present in both the plane wave and distorted wave calculations. In addition, although the minimum in the L=2 distribution at zero recoil momentum is somewhat filled in by the distortion, there remains a pronounced minimum. Thus, to emphasize clearly higher angular momentum states, the experiment must be biased toward larger recoil momentum. Similar distortion effects to those discussed above have also been pointed out by Chant [8] in an analysis of 100 MeV (p,pα) reactions.

In order to obtain some idea of the region of the nucleus which contributes most to the (p,pα) reaction, we have performed a series of calculations for the zero recoil momentum point with different radial cut-offs in the radial integral. By subtracting the cross sections for calculations of the zero recoil momentum point with different cut-off radii, we can obtain a reasonable estimate of the contribution for each radial region. This result is shown for the $^{24}Mg(p,p\alpha)^{20}Ne$ (0^+ ground state) reaction in Fig.12. Also shown in the figure is the α particle Woods-Saxon wave function, and the proton density distribution for ^{24}Mg obtained from electron scattering [19]. From this figure, we see that the reaction is strongly surface localized, and for zero recoil momentum the cross section results from α particles near the 3% nuclear density region. In this low density region, one might expect the concept of "pre-existing" α particles to be more meaningful . Such a concept would lead to higher cross sections. i.e. larger spectroscopic factors than predicted by normal shell model calculations. For larger values of the recoil momentum the same type of calculation shows that the reaction penetrates somewhat further into the nucleus, but still shows the dominance of the surface region. Thus, at least for small recoil momenta where the L=0 contribution is largest, the (p,pα) reaction strongly reflects the asymptotic behavior of the bound α particle wave function; i.e., the normalization and the separation energy.

Finally, to investigate the sensitivity of the theoretical momentum distributions to various ingredients in the calculations, we have performed a series of calculations with different bound state well parameters (see table 5) and different optical potentials. Most of the calculations were carried out for the $^{24}Mg(p,p\alpha)^{20}Ne$ reaction for the central region presented in fig.13, since this is the region for which the data is best defined. Similar results were obtained for ^{40}Ca.

For the bound state well, several combinations of radius and diffuseness were used (r_0 = 1.04, 1.24, 1.44 ; a = 0.68, 0.78, 0.88), but preserving the 5S quantum numbers and the separation energy. As might be expected on the basis of fig.12, the magnitude of P(q) is quite sensitive to these changes, but the shape is not. For example, with the extreme change in radius (r_0 = 1.04 → 1.44, a = 0.78) the magnitude of P(0) changes by about a factor of four. By contrast the magnitude of the plane wave calculation at zero recoil momentum changes by only about 20%. These results again emphasize the absorption effects which localize the reaction to the surface, and as a result the magnitude of P(0) more closely (although not exactly) reflects the normalization of the asymptotic tail of the bound α particle. Since we do not have a good method for choosing the bound state well parameters, we are left with a rather large uncertainty in the magnitude of the theoretical P(q), which appears in the extracted spectroscopic factors. As stated previously, we have chosen to use well parameters related to elastic α scattering. In optical model analysis of lower energy elastic α scattering, in spite of the numerous ambiguities, one of the constant features of the analysis is the mean square radius (MSR) of the real optical potential[17]. Our parameters (r_0 = 1.24, a = 0.78) very nearly reproduce the extracted MSR for this region. Unfortunately, in the (p,pα) calculations different bound state potentials with the same MSR do not produce the same P(q) (see table 5). However, for a reasonable range of radii and diffusenesses which have the same MSR, we find that the magnitude of the theoretical P(q) varies only by about ±30% around the value we have used. Thus the use of this MSR prescription does greatly reduce the possible variations in the magnitude. Obviously, one needs a better method of generating the α particle wave function. However, we hope that the use of this MSR procedure will at least allow us to extract reasonable spectroscopic information, particularly in terms of relative spectroscopic factors.

For the investigation of the sensitivity of the calculations to the optical potentials, we focused primarily on the α particle, on the assumption that the calculations are most sensitive to this potential. Also numerous ambiguities exist in the α potential, whereas the proton potentials are rather better known. For the ^{24}Mg(p,pα)^{20}Ne (0^+) reaction seven different α potentials were tried, three from the article of Singh et al.[17] corresponding to two different families, and four from the analysis of Mc Fadden and Satchler[19] of 24 MeV α scattering on ^{24}Mg corresponding to four different families. As in the case of the bound state investigation, the shape of P(q) for the region shown in fig.13 is not strongly dependent on the α optical potential. For example the half width at one quarter the maximum changes by less than 10%. However, the magnitude at zero recoil momentum varies by approximately ±40% around the value given in table 3. In general the shallower potentials give rise to a larger P(q), and the deeper potentials to a smaller P(q). For the proton potentials, reasonable variations in the strengths of the real and imaginary parts of both channels give rise to less than a 20% effect. We would conclude that overall one might expect something like a ±50% variation of the magnitude of P(0) due to the use of different optical potentials.

From the above investigation of the sensitivity of the calculations, we would hope that the absolute spectroscopic factors extracted from experiment are good to roughly a factor of two, although this might be very dependant upon the treatment of the bound α particle wave function. However, we expect the relative spectroscopic factors for different nuclei to be considerably better determined, since we have tried to use consistent potentials for the calculations.

5 - Comparison of experiment with PWIA and DWIA. α spectroscopic factors

The DWIA calculations lead to the results presented in figs. 9 to 13, and table 3. The normalization, which provides the spectroscopic factors, is discussed in sect.5.2. We first compare the calculated and experimental shapes.

5.1. Shapes.

Examples of PWIA calculations are shown on figs.9 and 13 for the case of ^{24}Mg. The PWIA maximum cross-sections for the three s-d shell target nuclei are 15 to 25 times larger than those obtained by DWIA, and the deep minima of PWIA are washed-out by the distortion effects. The DWIA calculations give more reasonable fits to experiment but serious discrepancies remain, especially for the 2^+ states. One must recall that due to the different experimental conditions the distorted wave calculation does not lead to a single curve ; the experimental points must be compared with segments of different curves corresponding to the different distortion conditions. Due to code limitations no calculation is available for the 4^+ states.

Both PWIA and DWIA predict fairly well the ratio between the cross-sections of measurements 1 and 3 for ^{24}Mg and ^{40}Ca (see table 3). This ratio seems thus to depend only on the free p-α cross-sections and the kinematic factor of formula (2).

0^+ states.

The DWIA reproduces quite well the general shape of the data: the position of the maximum slightly shifted towards negative values of q_R; the FWHM between 130 and 140 MeV/c; the change of slope near -130 MeV/c corresponding to the rise of the second maximum of a 5S momentum distribution. It also predicts fairly well the behaviour of the results for the extra measurements performed at $\theta_p = 67.4°$ and $67.3°$ for ^{24}Mg and ^{40}Ca, in particular the attenuation factors for data at the same q_R. However, it does not reproduce the angular effect (in θ_α) in measurement 4 for ^{40}Ca.

2^+ states.

When one normalizes the DWIA calculations in the region of the DWIA maxima, one sees that the theoretical distribution for $|\vec{q}_R| > 80$MeV/c provides a fair fit to experiment. Thus the total widths of the distributions are more or less well reproduced. However, a serious discrepancy -about an order of magnitude- appears in the low $|\vec{q}_R|$ region for all three s-d shell nuclei. In particular the minimum predicted by DWIA does not show up in the experimental data which is rather flat (within experimental errors) at small $|\vec{q}_R|$. Any undetected systematic error in the separation procedure of the 0^+ and 2^+ peaks could not account for such a large effect. The large values of $d^3\sigma$ at $|\vec{q}_R| \lesssim 80$ MeV/c could be due to a deficiency of the DWIA treatment or to other reaction mechanisms. We shall return to this problem in the conclusion section.

5.2. α spectroscopic factors.

The α spectroscopic factors S_α have been extracted for the 0^+ and 2^+ states of the s-d shell nuclei by normalizing the DWIA calculations to the experimental cross-sections in the region of the maxima of the theoretical distributions (i.e., 0-120 MeV/c for the 0^+ states ; 80-160 MeV/c for the 2^+ states). The absolute and relative values of S_α extracted in this way are listed in table 6. Relative values are obtained by setting S_α equal to unity for the transition $^{28}Si \rightarrow {}^{24}Mg$ (0^+ ground state). The errors indicated for S_α correspond to the experimental errors and to the extraction fitting procedure. The uncertainties involved in the DWIA calculations (choice of optical potentials and α particle bound state wave function parameters...) are not included. As discussed in Sect.4 these could amount to factors as large as 2 or 3. For this reason the relative values of S_α are probably more significant than the absolute ones.

We have obtained theoretical α-spectroscopic factors corresponding to a SU(3) description of the nuclei involved by combining the relative spectroscopic strengths calculated by Draayer[20] with the fractional parentage coefficients calculated by Hecht and Braunschweig[21]. These S_α are also listed in table 6. They were calculated for a pure SU(3) description. Configuration mixing in the s-d shell might change these figures by roughly 50% [22]. The SU(3) model should also provide a better description for nuclei in the first half of the s-d shell than for the ^{36}A and ^{40}Ca nuclei.

In table 6 one can see that on the average the absolute values of the S_α extracted from experiment are too large by about a factor of 3. The relative values however are in good agreement with the SU(3) predictions for the 2^+ final state for the ^{28}Si target and the 0^+ final state for the ^{24}Mg target. For the ^{40}Ca target the disagreement between the experimental and theoretical relative S_α is greater, but not unreasonable considering the size of the errors. The greatest discrepancy is for ^{24}Mg(p,pα)^{20}Ne(2^+). In this case,the SU(3) prediction is very low compared to experiment. It should not be forgotten, however, that in this case the extraction of the experimental S_α is quite difficult and the hypothesis underlying the fit might be questioned. Also if this spectroscopic factor is really very small as predicted by SU(3), the contribution from the simple quasi-free mechanism might be small compared to another mechanism which could be the cause of the difficulties at small $|\vec{q}_R|$ for the 2^+ states. Then the S_α extracted from experiment might be too large.

One may compare our results with those obtained from the study of the (^{6}Li,d) reaction at 32 and 36 MeV [23], the (d,^{6}Li) reaction at 35 and 55 MeV [24] and the (^{3}He,^{7}Be) reaction at 26, 30 and 41 MeV [25]. A conservative statement is that the differences between the (p,pα) and the transfer reaction results are not larger than the differences between the various transfer reaction results themselves. These differences can perhaps be traced back to the uncertainties involved in the DWIA or DWBA treatment. However, the relative $S_\alpha(0^+)$ for the ^{24}Mg target extracted from our (p,pα) data is in agreement with SU(3) and in disagreement with the value extracted from transfer reactions. For the ^{40}Ca target the $S_\alpha(0^+)$ disagree with SU(3) in both cases : this might correspond to a real structure effect. A recent (α,2α) experiment at 90 MeV [26] seems to give conflicting results ; however the DWIA analysis of these data does not seem very satisfactory as yet [8].

Only for the ^{40}Ca target do we observe an important excitation of the first 4^+ state, distinguishable by its contribution at very large $|\vec{q}_R|$. The reason for not observing a 4^+ excitation in the other two s-d targets might be due to the fact that $S_\alpha(4^+)$ is quite large for ^{40}Ca [9 times -i.e. (2J+1) times- the ground state spectroscopic factor] whereas it is much smaller for ^{24}Mg and ^{28}Si [about equal to $S_\alpha(0^+)$].

In the case of $^{58}_{28}Ni_{30}$ (p,pα) $^{54}_{26}Fe_{28}$, the cross-sections are very small, contrary to what could have been expected from some interpretations of recent experiments on hadron absorption by nuclei [4]. The reaction seems to lead mainly to excited states of the final nucleus ; this result can probably be related to the existence of a closed proton shell in the target nucleus and a closed neutron shell for the ground state of the final nucleus.

6. Conclusions

The (p,pα) reaction is especially sensitive to the surface region of the nucleus where α clustering might be important. This should show up in the size of the α spectroscopic factors. The agreement with the relative values of the SU(3) spectroscopic factors is quite good in a number of cases. It is certainly desirable to improve and extend the DWIA treatment of the (p,pα) reaction, in particular for the 2^+ and 4^+ states.

The (p,pα) reaction at 157 MeV exhibits a clear symmetry around the quasi-free kinematic conditions. This fact, along with the good agreement with the DWIA shape observed for the "ground state + ground state" transition provides evidence for the dominance of the quasi-free mechanism in the reaction. However the absence of a minimum at small $|\vec{q}_R|$ for the transitions leading to the 2^+ states raises the question as to the importance of contributions of other types of quasi-free mechanisms. For example, the reaction could proceed through the knock-out in the intermediate state of two protons and two neutrons with quantum numbers J=2, L=0, the interaction at the upper vertex giving rise to a real free α particle in the exit channel (see diagram on fig.2). A two step mechanism proceeding through a knock-out leading to the 0^+ ground state of the final nucleus followed by an excitation of the first 2^+ state through inelastic scattering of the outgoing α particle should also be considered.

Acknowledgments

We wish to thank M. Bernas who participated to the early stage of this experiment preparing the ^{4}He target with the help of M.Mommejat. We are very much indebted to N.S. Chant for the use of his D.W.I.A. code and to K.T. Hecht for putting his results at our disposal prior to publication. It is a pleasure to acknowledge fruitful discussions with V.V. Balashov, V. Gillet, I.E. McCarthy, D.J. Millener, V.G. Neudatchin and I. Rotter.

We are very grateful to Y. Bisson, R. David-Boyer, P. Lelong and F. Reide for their very efficient technical help ; we also wish to acknowledge the collaboration of the crews of the synchrocyclotron and of the IBM (Ariel) and UNIVAC computers.

REFERENCES

1 - V.V. BALASHOV, A.N. BOYARKINA and I. ROTTER, Nuclear Physics 59 (1964) 417.
- I. ROTTER, Fortschritte der Physik 16 (1968) 195.
- D. KURATH, Physical Review C7 (1973) 1390.

2 - V. GILLET, Proceedings of the "Second Int. Conf. on Clustering Phenomena in Nuclei", Univ. of Maryland (1975) 23.

3 - D.H. WILKINSON, Proceedings of the "Rutherford Jubilee International Conference", Univ. of Manchester (1961) 339.

4 - J.P. SCHIFFER, Proceedings of the "Second Int. Conf. on Clustering Phenomena in Nuclei", Univ. of Maryland (1975) 329, and references therein.

5 - Y. SAKAMOTO, Nuclear Physics 66 (1965) 531.

6 - A.M. CORMACK, J.N. PALMIERI, N.F. RAMSEY and R. WILSON, Physical Review 115 (1959) 599.

7 - D.F. JACKSON, Nuovo Cimento 40B (1965) 109 ;
Proc. Phys. Soc. 88 (1965) 101.

8 - N.S. CHANT and P.G. ROOS, Proceedings of the "Second Int. Conf. on Clustering Phenomena in Nuclei", Univ. of Maryland (1975) 255.

9 - V.M. KOLYBASOV, G.A. LEKSIN and I.S. SHAPIRO, ITEP 97 (1973).

10 - N.F. GOLOVANOVA, I.M. ILIN, Yu.F. SMIRNOV and V.G. NEUDATCHIN, JETP Letters 20 (1974) 310.
- V.V. BALASHOV, Proceedings of the "Second Int. Conf. on Clustering Phenomena in Nuclei", Univ. of Maryland (1975) 281.
- V.V. BALASHOV and V.N. MILEEV, Nuclear Physics (to be published).

11 - A.N. JAMES and H.G. PUGH, Nuclear Physics 42 (1963) 441.
- B. GOTTSCHALK and S. KANNENBERG, Physical Review C2 (1970) 24.
- R. BHOWMICK, C.F. BURDZIK, C.C. CHANG, N.S. CHANT, V.K.C. CHANG, A.A. COWLEY, J. CRAIG, D.A. GOLDBERG, H.D. HOLMGREN, K. KWIATKOWSKI, P.G. ROOS, W. REICHART, N.S. WALL and R. WOODY III, University of Maryland, Progress Report (1973) 97.
- The many references on ^{6}Li are not listed here.

12 - D. BACHELIER, M. BERNAS, O.M. BILANIUK, J.L. BOYARD, J.C. JOURDAIN and P. RADVANYI, Physical Review C7 (1973) 165.

13 - R. ANNE, P. DELPIERRE, A. DEVAUX, J. KAHANE, G. LANDAUD, R. SENE and J. YONNET, Contributed paper "Second Int. Conf. on Clustering Phenomena in Nuclei", Univ. of Maryland (1975) 309.
- R.I. STEINBERG, C.C. CHANG, N.S. CHANT, J.P. DIDELEZ, H.D. HOLMGREN, P.G. ROOS and J.S. WU, contributed paper "Second Int. Conf. on Clustering Phenomena in Nuclei", Univ. of Maryland (1975) 315.

14 - N.S. CHANT and P.G. ROOS, Progress Report, Univ. of Maryland, Cyclotron lab. (1974).

15 - G. JACOB and Th.A.J. MARIS, Rev. Mod. Phys. 38 (1966) 121 ;
Rev. Mod. Phys. 45 (1973) 6.

16 - V. COMPARAT, R. FRASCARIA, N. MARTY, M. MORLET et A. WILLIS, Nuclear Physics A221 (1974) 403.

17 - P.P. SINGH, R.E. MALMIN, M. HIGH and D.W. DEVINS, Physical Review Letters 23 (1969) 1124.

18 - H.H. CHANG and B.W. RIDLEY, Annual report, Univ. of Colorado (1971)55;
Annual report, Univ. of Colorado (1972)49.

19 - L. Mc FADDEN and G.R. SATCHLER, Nuclear Physics 84 (1966) 177.

20 - J.P. DRAAYER, Nuclear Physics A237 (1975) 157.

21 - K.T. HECHT and D. BRAUNSCHWEIG, Nuclear Physics A244 (1975) 365.

22 - J.B. Mc GRORY, Physics Letters 47B (1973) 481.
- A. ARIMA and D. STROTTMAN, Oxford Univ., Nucl. Phys. Theor. Gp. report n°46 (1973).

23 - N. ANANTARAMAN, C.L. BENNETT, J.P. DRAAYER, H.W. FULBRIGHT, H.E. GOVE and J. TOKE, Physical Review Letters 35 (1975) 1131.

24 - R.L. Mc GRATH, D.L. HENDRIE, E.A. Mc CLATCHIE, B.G. HARVEY and J. CERNY, Physics Letters 34B (1971) 259.

- F.D. BECCHETTI, L.T. CHUA, J. JANECKE and A.M. VAN DER MOLEN, Physical Review Letters 34 (1975) 225.

25 - G. AUDI, C. DETRAZ, M. LANGEVIN and F. POUGHEON, Nuclear Physics A237 (1975) 300, and references therein.
- W.F. STEELE, P.A. SMITH, J.E. FINCK and G.M. CRAWLEY, Annual report Michigan State Univ. (1975).

26 - J.D. SHERMAN, D.L. HENDRIE and M.S. ZISMAN, Contributed paper "Second Int. Conf. on Clustering in Nuclei", Univ. of Maryland (1975) 319.

TABLES

Table 1 : Kinematic characteristics of the various measurements. $q_R(0^+)$ and $q_R(2^+)$ correspond to the recoil nucleus momenta for the 0^+ ground state and the 2^+ first excited state respectively; q_R('4.4') corresponds to the 4.4 MeV group in the case of the ^{36}A recoil nucleus.
The sign convention is explained in section 3.3. θ_p, θ_α are in degrees , E_p in MeV , q_R in MeV/c.

Table 2 : Targets and experimental resolution achieved. The resolution is given for $\vec{q}_R \approx \vec{0}$ and $E^* = 0$.

Table 3 : General features of the experimental and calculated $d^3\sigma/dE_p\, d\Omega_p\, d\Omega_\alpha$ versus q_R, for the 0^+ ground state and the 2^+ first excited state, for ^{24}Mg, ^{28}Si and ^{40}Ca.
q_R(Maximum) and $d^3\sigma$(Maximum) correspond to the maximum value of $d^3\sigma$ obtained in the distribution ; q_R('1st maximum') and $d^3\sigma$('1st maximum') correspond to the region where $d^3\sigma$ is maximum for PWIA and DWIA, and the experimental $d^3\sigma$ given denotes the main value obtained in the same region.
The DWIA and PWIA values correspond to an α-spectroscopic factor of 1.

Table 4 : Optical potential parameters used in the DWIA calculations for the (p,pα) reactions.
V, r_0, a and W, r'_0, a' correspond to the real and imaginary part respectively ; units used are MeV and fm.

Table 5 : Bound state well parameters investigation for ^{24}Mg(p,pα)^{20}Ne(0^+). r_0 and a are the given radius and diffuseness. MSR is the calculated mean square radius of the real optical potential.

Table 6 : α spectroscopic factors for $^{24}Mg \rightarrow {}^{20}Ne+\alpha$, $^{28}Si \rightarrow {}^{24}Mg+\alpha$ and $^{40}Ca \rightarrow {}^{36}A+\alpha$ for the 0^+ ground state and the 2^+ first excited state of the final nucleus.

Absolute values are extracted from the DWIA analysis and calculated from pure SU(3) configurations ; relative values, normalized to S_α for $^{28}Si \rightarrow {}^{24}Mg(0^+)+\alpha$, are also given.

Sixfold measurement number	$^{40}Ca(p,p\alpha)^{36}A$					
	θ_p	θ_α	E_p	$q_R(0^+)$	$q_R(2^+)$	$q_R('4.4')$
1	60.0	50.6	105.8	- 56	- 43	- 27
			109.3	- 30	- 17	+ 2
			112.7	- 8	+ 12	+ 30
		65.6	105.8	-160	-154	-148
			109.3	-143	-139	-136
			112.7	-131	-129	+130
2	60.0	48.0	95.3	-128	-116	-101
			98.4	-107	- 95	- 80
			101.5	- 86	- 74	- 58
		63.0	95.3	-201	-193	-183
			98.4	-182	-173	-164
			101.5	-162	-155	-146
3	67.3	47.2	105.8	- 3	+ 11	+ 29
			[illegible]	+ 26	+ 39	+ 57
			112.7	+ 54	+ 68	+ 87
		62.2	105.8	-147	-146	+147
			109.3	+140	+142	+146
			112.7	+139	+144	+152
4	60.0	43.5	107.6	- 76	- 69	- 62
			111.1	- 71	- 68	+ 69
			114.5	+ 76	+ 78	+ 86
		58.5	107.6	- 90	- 84	- 78
			111.1	- [illegible]2	- 69	+ 70
			114.5	+ 63	+ 66	+ 75

Sixfold measurement number	$^{24}Mg(p,p\alpha)^{20}Ne$				
	θ_p	θ_α	E_p	$q_R(0^+)$	$q_R(2^+)$
1	60.0	50.1	103.8	- 56	- 45
			107.2	- 30	- 19
			110.6	- 8	+ 10
		64.8	103.8	-156	-151
			107.2	-140	-136
			110.6	-127	-126
2	60.0	47.9	91.9	-136	-127
			95.0	-116	-106
			98.1	- 95	- 85
		62.6	91.9	-209	-202
			95.0	-189	-183
			98.1	-170	-164
3	67.4	47.7	103.8	- 8	
			107.2	+ 24	
			110.6	+ 52	

Sixfold measurement number	$^{28}Si(p,p\alpha)^{24}Mg$				
	θ_p	θ_α	E_p	$q_R(0^+)$	$q_R(2^+)$
1	60.0	50.0	103.3	- 56	- 47
			106.6	- 30	- 21
			110.0	- 8	+ 9
		65.0	103.3	-158	-155
			106.6	-142	-140
			110.0	-130	-129
2	60.0	47.5	93.6	-121	-113
			96.6	-101	- 93
			99.7	- 81	- 72
		62.5	93.6	-195	-190
			96.6	-176	-171
			99.7	-158	-153

$^{58}Ni(p,p\alpha)^{54}Fe$				
θ_p	θ_α	E_p	$q_R(0^+)$	$q_R(2^+)$
60.0	50.7	106.4	- 56	- 47
		109.8	- 30	- 20
		113.3	- 8	+ 10
	65.7	106.4	-160	-156
		109.8	-144	-141
		113.3	-131	-130

Table 1

Target	Enrichment (%)	Thickness ($mg.cm^{-2}$)	Resolution at (0,0) ΔE** (MeV)	$\Delta\vert\vec{q}_R\vert$ (MeV/c)
^{4}He	natural	0.35	2.0	
^{6}Li	99.3	9.6	2.6	
^{24}Mg	99.6	15.4	2.4	30
	natural	11.6		
^{28}Si	natural(92.2)	13.3	2.9	31
^{40}Ca	natural(96.9)	13.1	2.8	31
		6.5	2.3	24
^{58}Ni	99.8	11.15	2.5	30

Table 2.

		0^+ ground state of final nucleus				2^+ first excited state of final nucleus		
		q_R (Maximum) (MeV/c)	$d^3\sigma$ (Maximum) ($\mu b.MeV^{-1}.sr^{-2}$)	FWHM (MeV/c)	$\frac{d^3\sigma(Mes1)}{d^3\sigma(Mes3)}$	q_R ("1st Maximum") (MeV/c)	$d^3\sigma$ ("1st Maximum") ($\mu b.MeV^{-1}.sr^{-2}$)	FWHM (MeV/c)
^{24}Mg target	Experiment	- 20	2.5 ± 0.5	80	$2.^{+1.4}_{-0.6}$		0.22 ± 0.11	220
	DWIA	- 10	8.8	134	1.8	-120	0.98	340
	PWIA	0	137.	113	2.1	-140	13.4	370
^{28}Si target	Expe iment	0	1.6 ± 0.3	110			0.25 ± 0.09	280
	DWIA	- 10	5.4	136		-120	0.66	340
	PWIA	0	130	101		-140	13.0	360
^{40}Ca target	Experiment	- 20	2.5 ± 0.4	110	$1.3^{+0.4}_{-0.3}$		0.39 ± 0.12	250
	DWIA	- 15	5.2	134	1.9	-130	0.60	350
	PWIA	0	132.	104	2.1	-130	12.8	350

Table 3.

Optical potential parameters	$^{24}Mg(p,p\alpha)^{20}Ne$ $^{28}Si(p,p\alpha)^{24}Mg$			$^{40}Ca(p,p\alpha)^{36}A$		
	Incoming proton	Outgoing proton	Outgoing alpha	Incoming proton	Outgoing proton	Outgoing alpha
V	12.3	23.3	96.0	14.1	25.0	124.2
W	14.0	12.0	47.9	14.0	12.0	10.0
r_0	1.43	1.43	1.40	1.38	1.38	1.10
a	0.62	0.62	0.71	0.59	0.59	0.95
r'_0	1.15	1.15	1.40	1.18	1.18	1.84
a'	0.63	0.63	0.71	0.60	0.60	0.49

Table 4.

r_0 (fm)	a (fm)	$d^3\sigma_{DWIA}$ (a.u.)	MSR (fm^2)
1.04	0.78	1.16	13.18
1.24	0.68	1.61	13.19
1.24	0.78	2.50	15.20
1.24	0.88	3.71	17.48
1.44	0.78	4.86	17.57

Table 5.

State of final nucleus	0^+ ground state			2^+ first excited state		
Target nucleus	^{24}Mg	^{28}Si	^{40}Ca	^{24}Mg	^{28}Si	^{40}Ca
DWIA extracted S_α	0.23±0.07	0.24±0.05	0.50±0.07	0.2±0.1	0.4±0.1	0.9±0.4
SU(3) calculated S_α	0.08	0.09	0.09	0.01	0.11	0.45
Relative S_α(DWIA)	$1.0^{+0.4}_{-0.4}$	1	$2.1^{+0.5}_{-0.5}$	$0.9^{+0.5}_{-0.4}$	$1.5^{+0.5}_{-0.4}$	$3.8^{[illegible]}_{[illegible]}$
Relative S_α(SU(3))	[illegible]	1	1.0	0.1	1.2	5.0

Table 6.

FIGURE CAPTIONS

Fig.1. Kinematics of the (p,pα) reaction.

The subscripts o, p, α, R correspond to the incoming proton, the outgoing proton, the outgoing alpha particle and the recoil nucleus respectively.

The endpoint of $\vec{q}_R$ follows a straight line Δ parallel to the direction of $\vec{p}_\alpha$.

Fig.2. First order diagram for the quasi-free (p,pα) reaction.

Fig.3. Experimental set-up.

Fig.4. $|\vec{q}_R|$ (E^*) and $\vec{q}_R(\theta)$ representations for the $^{28}Si(p,p\alpha)^{24}Mg$ measurements.

The notations A, B, C, Tel 1 and Tel 2 correspond to the telescopes shown on figure 3 ; θ_{α_1} and θ_{α_2} give the directions of $\vec{p}_\alpha$ for Tel 1 and Tel 2 respectively.

The solid curves correspond to measurement 1 ; the 0^+ ground state and the 2^+ first excited state are indicated by circles and stars respectively ; on the (E^*, $|\vec{q}_R|$) map, dashed lines correspond to measurement 2. See also table 1.

Fig.5. Averaged excitation energy spectra $d^4\sigma/dE_p d\Omega_p dE_\alpha d\Omega_\alpha$ for $|\vec{q}_R|$ intervals 0-100 and 100-200 MeV/c, for ^{24}Mg and ^{28}Si target nuclei.

The positions of the 0^+ ground state and 2^+ first excited state are indicated by arrows.

Fig.6. Averaged excitation energy spectra $d^4\sigma/dE_p d\Omega_p dE_\alpha d\Omega_\alpha$ for $|\vec{q}_R|$ intervals 0-100, 100-220, 60-90 and 0-220 MeV/c for the ^{40}Ca target nucleus.

The positions of the 0^+ ground state, 2^+ first excited state and the 4.4 MeV group are indicated by arrows.

Fig.7. Averaged excitation energy spectrum $d^4\sigma/dE_p d\Omega_p dE_\alpha d\Omega_\alpha$ for the total 0-220 MeV/c $|\vec{q}_R|$ interval for the ^{58}Ni target nucleus.

Fig.8. Elementary excitation energy spectra.
Spectra are identified by the target nucleus. The $^4He(p,p)^4He$ and $^6Li(p,p\alpha)^2H$ spectra, which indicate the resolution of the experiment (see table 2), are given for comparison. The ^6Li spectrum is taken from our previous experiment (ref.12). q_D is the recoil momentum for the 0^+ ground state, indicated as $q_R(0^+)$ in table 1 ; level positions are indicated by arrows ('4.4' denotes the group of levels of ^{36}A around 4.4 MeV) ; the dashed lines correspond to a fit with gaussian shapes.

Fig.9. $d^3\sigma/dE_p\ d\Omega_p\ d\Omega_\alpha$ versus q_R for $^{24}Mg(p,p\alpha)^{20}Ne$.
0^+ denotes the ground state, 2^+ the 1.63 MeV first excited state of ^{20}Ne ; the thin curves correspond to PWIA calculations ; the other curves and symbols are explained in the caption of fig.11.

Fig.10. $d^3\sigma/dE_p\ d\Omega_p\ d\Omega_\alpha$ versus q_R for $^{28}Si(p,p\alpha)^{24}Mg$.
0^+ denotes the ground state, 2^+ the 1.37 MeV first e[illegible] state of ^{24}Mg ; the curves and symbols are explained in the c[illegible] of fig.11.

Fig.11. $d^3\sigma/dE_p\ d\Omega_p\ d\Omega_\alpha$ versus q_R for $^{40}Ca(p,p\alpha)^{36}A$.
0^+ denotes the ground state, 2^+ the 1.97 MeV first excited state, '4.4 MeV', the 4.4 MeV group of excited states of ^{36}A.
The sign of q_R is defined in section 3.3. Closed (open) circles and triangles correspond to measurements 1(2) and 3(4) respectively.
The thick curves correspond to the DWIA results : solid lines for measurements 1 and 2 ; dashed lines for measurement 3 ; point-dashed lines for measurement 4.
These DWIA curves correspond to the spectroscopic factors listed in table 7.

Fig.12. Plots of the radial dependence of various quantities for ^{24}Mg. The top panel shows the radial wave function assumed for the α particle in ^{24}Mg which was used in the Impulse Approximation calculations ($\int_0^\infty u^2\,dr = 1$).
The middle panel indicates the contribution to the DWIA cross-section for each 0.5 fm interval of the radial integral (see section 4).
The bottom panel shows the charge distribution of ^{24}Mg measured in electron scattering (ref.19).

Fig.13. Calculated momentum distributions P(q) for $^{24}Mg(p,p\alpha)^{20}Ne$, with angular conditions $\theta_p = 60.0$ and $\theta_\alpha = 50.1$ degrees. The thick curves correspond to the Distorted Wave calculation ; the dashed curves correspond to the Plane Wave calculation normalized to the Distorted Wave result by the factor indicated. 0^+ denotes the ground state, 2^+ the 1.63 MeV first excited state of ^{20}Ne.

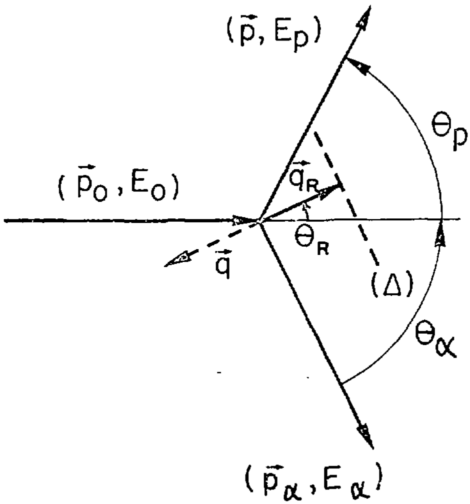

$(\vec{p}, E_p)$
Θ_p
$(\vec{p}_0, E_0)$
$\vec{q}_R$
Θ_R
$\vec{q}$
(Δ)
Θ_α
$(\vec{p}_\alpha, E_\alpha)$

fig.1

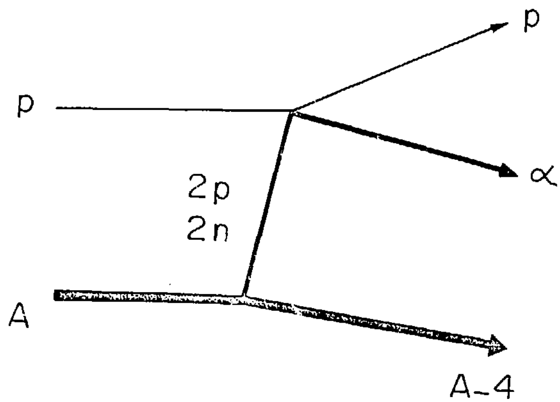

fig.2

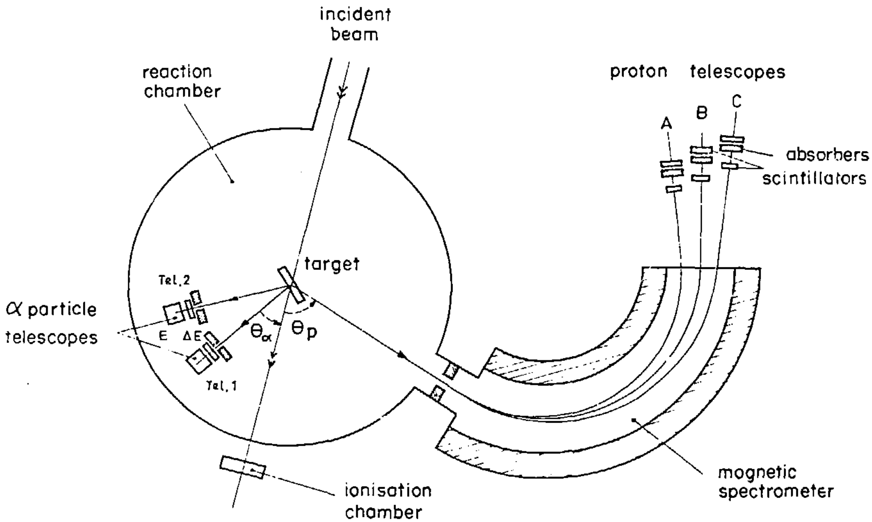
incident beam
reaction chamber
proton telescopes
A
B
C
absorbers
scintillators
target
Tel.2
α particle telescopes
E
ΔE
Θα
Θp
Tel.1
ionisation chamber
magnetic spectrometer

fig.3

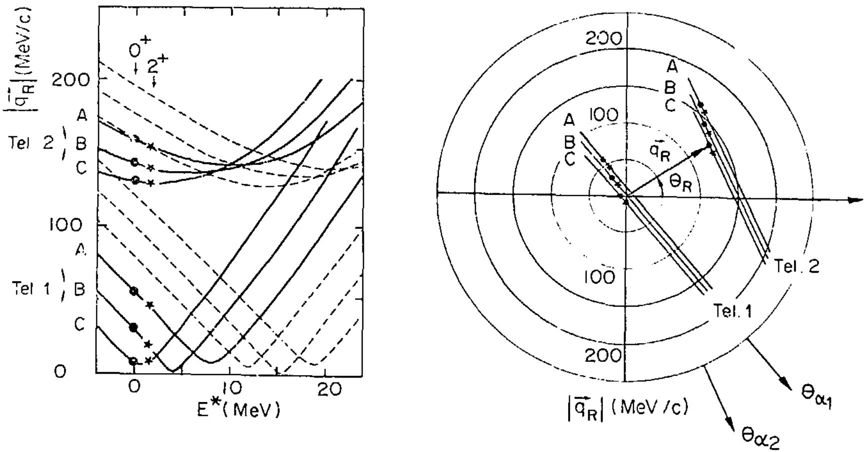

0+
2+
200
A
Tel 2
B
C
100
A
Tel 1
B
C
0
0
10
20
E*(MeV)
|q_R| (MeV/c)
200
100
A
B
C
A
B
C
100
q_R
θ_R
Tel. 2
100
Tel. 1
200
θα1
θα2
|q_R| (MeV/c)

Fig. 4

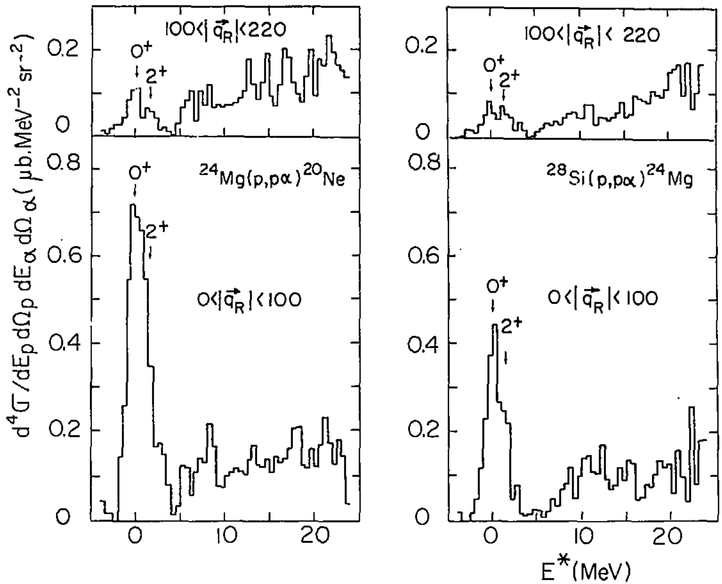
100<|$\vec{q}_R$|<220
0⁺
2⁺
$^{24}Mg(p,p\alpha)^{20}Ne$
0<|$\vec{q}_R$|<100
$^{28}Si(p,p\alpha)^{24}Mg$
$d^4\sigma/dE_p d\Omega_p dE_\alpha d\Omega_\alpha$ ($\mu b.MeV^{-2} sr^{-2}$)
E* (MeV)
0
0.2
0.4
0.6
0.8
10
20

fig.5

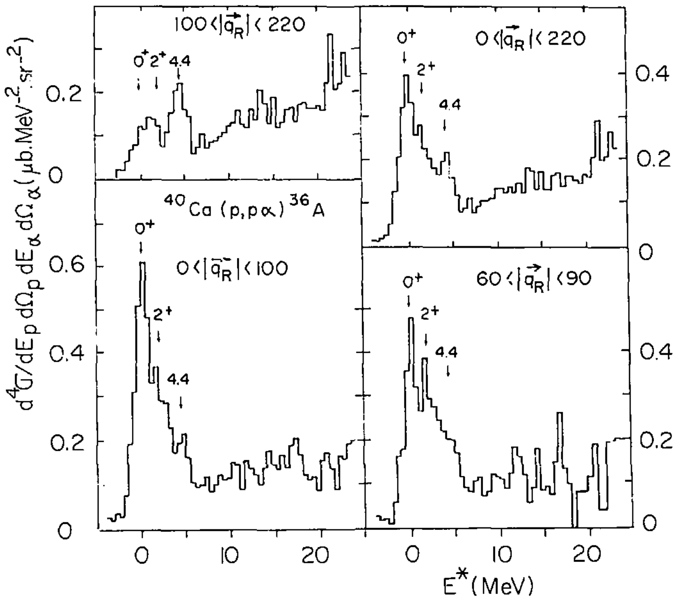

100 < |$\vec{q}_R$| < 220
0 < |$\vec{q}_R$| < 220
^{40}Ca (p,pα) ^{36}A
0 < |$\vec{q}_R$| < 100
60 < |$\vec{q}_R$| < 90
0$^+$
2$^+$
4.4
$d^4\sigma/dE_p\,d\Omega_p\,dE_\alpha\,d\Omega_\alpha$ (μb.MeV^{-2}.sr^{-2})
E* (MeV)
0
0.2
0.4
0.6
10
20

fig.6

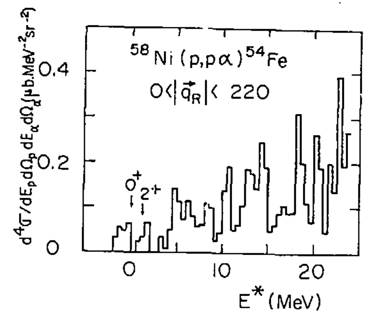

58 Ni (p,pα) 54 Fe
0 < |q_R| < 220
0+
2+
0.4
0.2
0
0
10
20
E* (MeV)
d4σ/dEp dΩp dEα dΩα (μb.MeV-2 sr-2)

fig.7

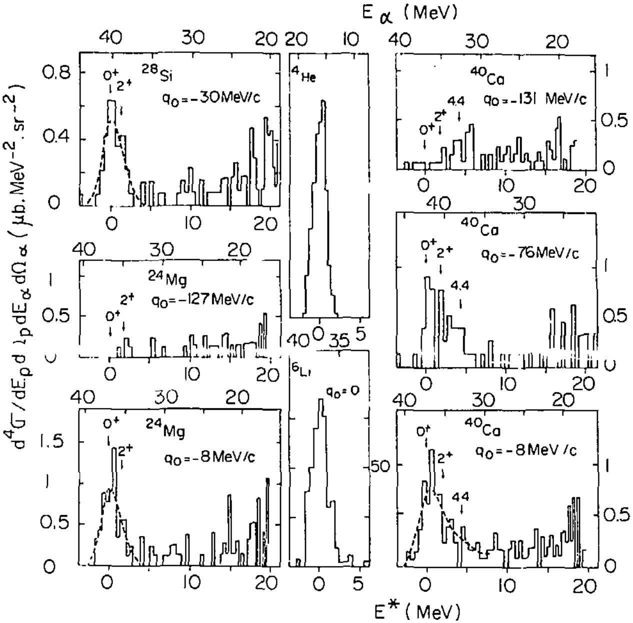

E α (MeV)
E* (MeV)
d4σ/dEp dΩp dEα dΩα (μb.MeV-2.sr-2)
28Si
q0=-30MeV/c
4He
40Ca
q0=-131 MeV/c
24Mg
q0=-127MeV/c
q0=-76MeV/c
6Li
q0=0
q0=-8MeV/c
q0=-8MeV/c

fig.8

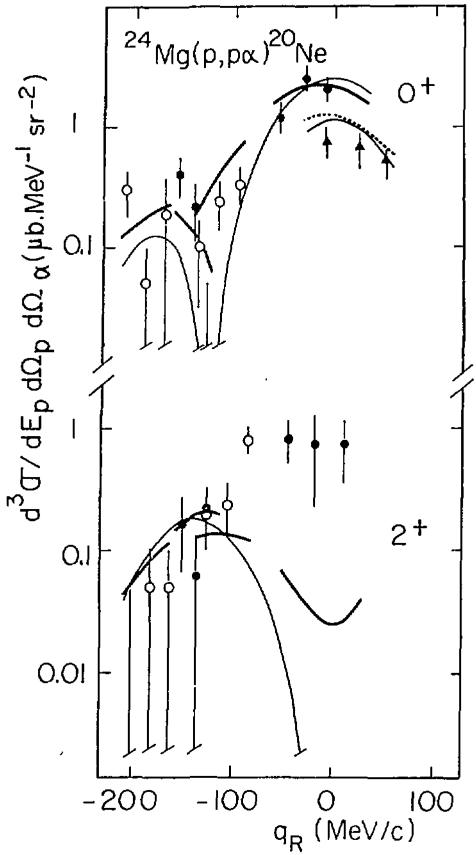
$^{24}Mg(p,p\alpha)^{20}Ne$
0^+
2^+
$d^3\sigma/dE_p\,d\Omega_p\,d\Omega_\alpha\,(\mu b.MeV^{-1}\,sr^{-2})$
1
0.1
1
0.1
0.01
-200
-100
0
100
q_R (MeV/c)

fig.9

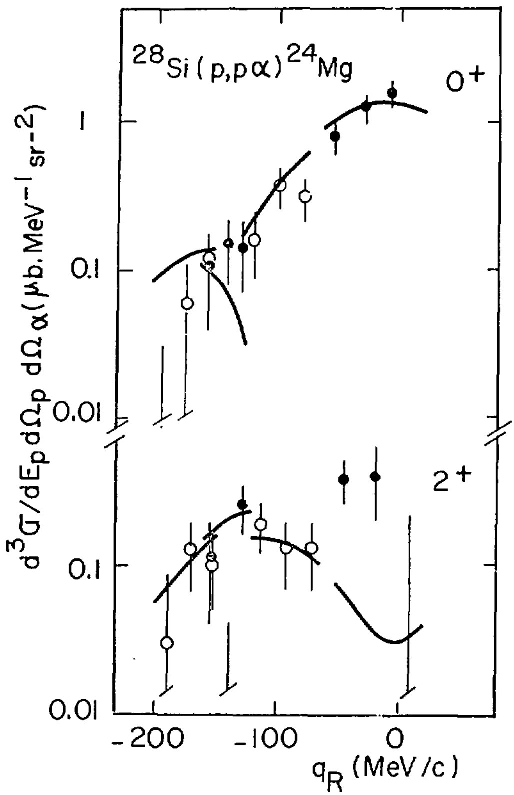

$^{28}Si(p,p\alpha)^{24}Mg$
0^+
2^+
1
0.1
0.01
0.1
0.01
$d^3\sigma/dE_p d\Omega_p d\Omega_\alpha (\mu b. MeV^{-1} sr^{-2})$
-200
-100
0
q_R (MeV/c)

fig.10

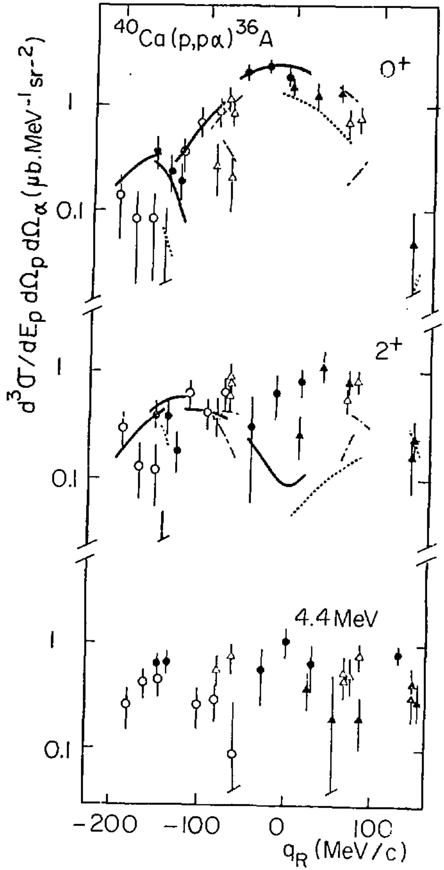

$^{40}Ca(p,p\alpha)^{36}A$
0^+
2^+
4.4 MeV
$d^3\sigma/dE_p\,d\Omega_p\,d\Omega_\alpha$ (μb.MeV^{-1}sr^{-2})
1
0.1
1
0.1
1
0.1
−200
−100
0
100
q_R (MeV/c)

fig.11

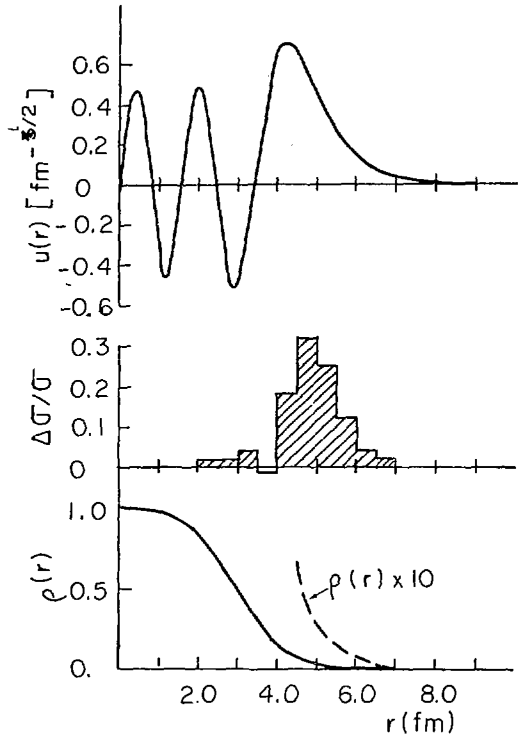

0.6
0.4
0.2
0
-0.2
-0.4
-0.6
u(r) [fm$^{-3/2}$]
0.3
0.2
0.1
0
Δσ/σ
1.0
ρ(r)
0.5
0.
ρ(r) x 10
2.0
4.0
6.0
8.0
r (fm)

fig. 12

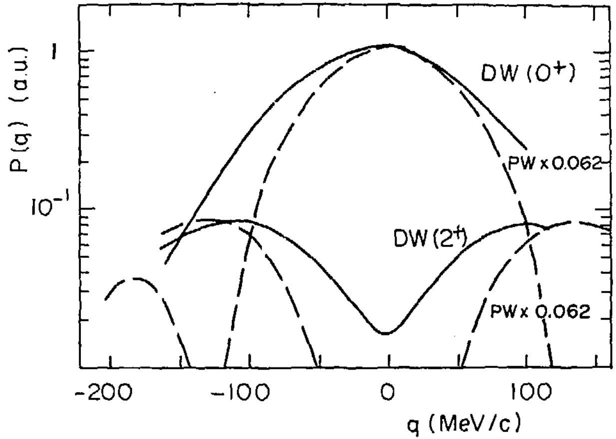

fig.13